UC-34D
LBL-18408
Preprint c.1

Lawrence Berkeley Laboratory

UNIVERSITY OF CALIFORNIA

RECEIVED
LAWRENCE
BERKELEY LABORATORY

DEC 19 1984

LIBRARY AND
DOCUMENTS SECTION

Physics Division

Submitted for publication

TESTS OF MODELS FOR QUARK AND GLUON FRAGMENTATION IN e^+e^- ANNIHILATION $\sqrt{s} = 29$ GeV

PEP-4 TPC Collaboration

October 1984

For Reference
Not to be taken from this room

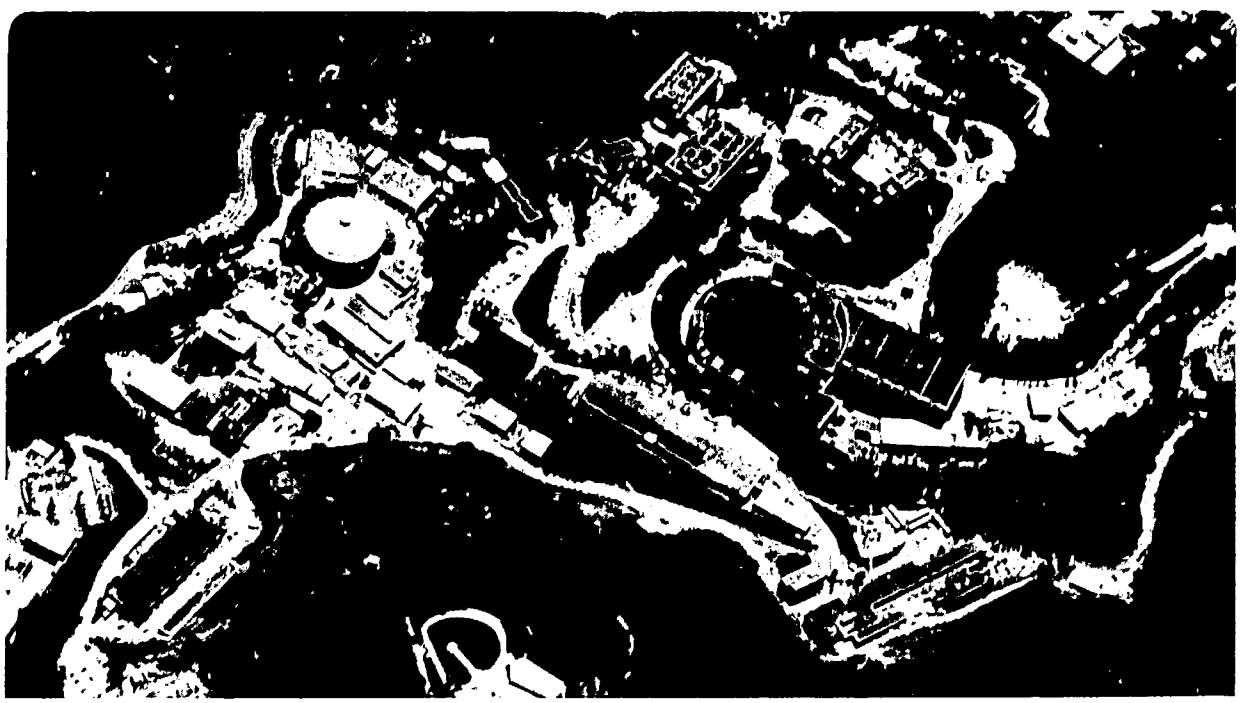

LBL-18408 c.1

Prepared for the U.S. Department of Energy under Contract DE-AC03-76SF00098

DISCLAIMER

This document was prepared as an account of work sponsored by the United States Government. While this document is believed to contain correct information, neither the United States Government nor any agency thereof, nor the Regents of the University of California, nor any of their employees, makes any warranty, express or implied, or assumes any legal responsibility for the accuracy, completeness, or usefulness of any information, apparatus, product, or process disclosed, or represents that its use would not infringe privately owned rights. Reference herein to any specific commercial product, process, or service by its trade name, trademark, manufacturer, or otherwise, does not necessarily constitute or imply its endorsement, recommendation, or favoring by the United States Government or any agency thereof, or the Regents of the University of California. The views and opinions of authors expressed herein do not necessarily state or reflect those of the United States Government or any agency thereof or the Regents of the University of California.

LBL-18408
TPC-LBL-84-45

Tests of Models for Quark and Gluon Fragmentation in e^+e^- Annihilation $\sqrt{s}$ =29 GeV

H. Aihara[6], M. Alston-Garnjost[1], J.A. Bakken[4], A. Barbaro-Galtieri[1], A.V. Barnes[1], B.A. Barnett[4], H.-U. Bengtsson[2], B.J. Blumenfeld[4], A.D. Bross[1], C.D. Buchanan[2], O. Chamberlain[1], C-Y. Chien[4], A.R. Clark[1], A. Cordier[1], O.I. Dahl[1], C.T. Day[1], K.A. Derby[1], P.H. Eberhard[1], D.L. Fancher[1], H. Fujii[6], T. Fujii[6], B. Gabioud[1], J.W. Gary[1], W. Gorn[3], N.J. Hadley[1], J.M. Hauptman[1], W. Hofmann[1], J.E. Huth[1], J. Hylen[4], T. Kamae[6], H.S. Kaye[1], R.W. Kenney[1], L.T. Kerth[1], R.I. Koda[2], R.R. Kofler[5], K.K. Kwong[3], J.G. Layter[3], C.S. Lindsey[3], S.C. Loken[1], X.Q. Lu[4], G.R. Lynch[1], L. Madansky[4], R.J. Madaras[1], K. Maruyama[6], J.N. Marx[1], J.A.J. Matthews[4], S.O. Melnikoff[3], W. Moses[1], P. Nemethy[1], D.R. Nygren[1], P.J. Oddone[1], D.A. Park[2], A. Pevsner[4], M. Pripstein[1], P.R. Robrish[1], M.T. Ronan[1], R.R. Ross[1], F.R. Rouse[1], R.R. Sauerwein[1], G. Shapiro[1], M.D. Shapiro[1], B.C. Shen[3], W.E. Slater[2], M.L. Stevenson[1], D.H. Stork[2], H.K. Ticho[2], N. Toge[6], R.F. van Daalen Wetters[2], G.J. VanDalen[3], R. van Tyen[1], E.M. Wang[1], M.R. Wayne[2], W.A. Wenzel[1], H. Yamamoto[6], M. Yamauchi[6], W-M. Zhang[4]

[1]Lawrence Berkeley Laboratory, University of California, Berkeley, CA 94720,
[2]University of California, Los Angeles, CA 90024,
[3]University of California, Riverside, CA 92521,
[4]Johns Hopkins University, Baltimore, MD 21218,
[5]University of Massachusetts, Amherst, MA 01003,
[6]University of Tokyo, Tokyo 113, JAPAN

October 1984

Abstract

Three currently used fragmentation models are tested by studying the distribution of particles between jet axes in the 3-jet events of e^+e^- annihilation, using data collected by the Time Projection Chamber at PEP. These three models – the Lund String model, the Webber Cluster model and an Independent Fragmentation model (IF) – each implement different Lorentz-frame structures for the fragmentation process of quarks and gluons into hadrons. The Lund model provides a good description of the data, while the IF model does not. The Webber model, which is untuned, does not describe the absolute particle densities between jets, but correctly predicts the ratios of those densities, which are less sensitive to the tuning.

1 *Introduction*

Quantum Chromodynamics (QCD) successfully accounts for many features of high energy e^+e^- annihilation data; e.g. jet broadening, violation of scaling in inclusive particle distributions and approximate KNO scaling[1]. However, since the non-perturbative structure of QCD is unknown, it does not predict how partons fragment into hadrons. Tests of QCD, therefore, depend upon phenomenological models to unfold the fragmentation process. Thus it is necessary to test these models before perturbative quantities, such as the strong coupling constant α_S, can be reliably measured. In addition, tests of these models can contribute to a better understanding of the hadronization process itself.

According to the quark-parton model, hadron production in e^+e^- annihilations occurs through the formation of a virtual photon or Z^o boson which subsequently decays into a quark-antiquark pair. "Traditional" fragmentation models evolve the $q\bar{q}$ pair, using $1st$ or $2nd$ order QCD, into a configuration of partons. A confinement scheme is implemented to describe the transition from partons to hadrons. The use of finite order QCD implies that the parton evolution is terminated at early times, leaving confinement schemes to deal with the hadronization of large mass systems. Examples are the Lund String Fragmentation model (SF) [2], in which a color flux tube (string) connects the partons, and the Ali [3] and Hoyer [4] Independent Fragmentation models (IF), in which partons fragment in isolation from each other. More recently, QCD motivated Cluster Fragmentation models (CF) have become available [5,6,7]. These models continue the parton evolution through a leading-log QCD quark-gluon shower until all partons are nearly on their mass shell. The partons form low mass color-singlet clusters which decay into hadrons according to

2-body phase space or through a parameterization of low energy data.

Differences between these models can appear in their predictions for the angular distribution of particles in 3-jet events, in which the initial q or $\overline{q}$ radiates a hard acolinear gluon. These differences arise as a consequence of the Lorentz-frame structures for the fragmentation process in each model. Consider the situation illustrated in Figure 1. In the Lund SF model, a string stretches from the quark to the antiquark through the gluon. The qg and $\overline{q}g$ string segments each fragment in their respective rest frames, thus serving as sources of the observed hadrons (Figure 1(a)). Fragmentation products appear boosted because these sources are in motion with respect to the overall center-of-mass. As a consequence, the region between the q and $\overline{q}$ is depleted of particles relative to the qg or $\overline{q}g$ regions. Due to its boost origin, this asymmetry is enhanced by selecting particles with a large energy relative to momentum in the event plane, i.e. heavy particles such as kaons and protons or particles with a large momentum component out of the event plane. In IF models, the fragmentation frame coincides with the overall center-of-mass. Thus partons fragment with an azimuthal symmetry and no $q-\overline{q}$ region depletion appears (Figure 1(b)). CF models can exhibit an asymmetry similar to that of the SF model because, as in the SF model, the rest frames of the hadron sources (in this case, clusters) are in motion (Figure 1(c)). Not all CF models can be expected to demonstrate such an asymmetry, however, because – depending upon the specific CF model under consideration – clusters may or may not preferentially populate the qg and $\overline{q}g$ regions.

In this paper, we present tests of fragmentation models using particle distributions in 3-jet events recorded by the Time Projection Chamber (TPC) detector at

PEP. Earlier, the JADE collaboration has presented evidence that particle distributions in 3-jet events prefer SF, as opposed to IF, models, using $1st$ order QCD [8]. However, there has been no confirmation of their results until now. We extend the analysis for these traditional models to $2nd$ order QCD and in addition examine CF models. An important aspect of the analysis is the behavior of the heavy particles relative to the light: we use the superior particle identification capabilities of the TPC for this purpose.

Our results are based on 29,000 e^+e^- hadronic annihilation events recorded by the TPC at $\sqrt{s} = 29$ GeV, corresponding to an integrated luminosity of $77pb^{-1}$. The TPC detector, its subsystems and the selection criteria for hadronic events have been described in detail elsewhere [9,10] The present analysis makes use of charged particles recorded by the central Time Projection Chamber and photons recorded by the barrel Hexagonal Calorimeter (HEX). Charged particles are identified through a simultaneous measurement of momentum and dE/dx energy loss. The momentum resolution is typically $(dp/p)^2 = (0.06)^2 + (0.035p)^2$, with p in GeV/c. The dE/dx resolution of 3.7% results in a pion-kaon separation of more than 3 standard deviations for particle momenta above 2.0 GeV/c, or below 0.9 GeV/c. Low momentum cutoffs of .15, .35 and .45 GeV/c are imposed by energy loss in the material before the TPC, for charged pions, kaons and protons, respectively. The HEX is a 10 r.l. thick lead gas-sampling Geiger mode calorimeter [11] which records photons with energies larger than .40 GeV. Its single photon energy resolution is $16\%/\sqrt{E\,(GeV)}$.

The remaining sections are organized as follows. In section 2 we introduce the fragmentation models and their optimizations for this analysis. In section 3 we

discuss the 3-jet event selection and particle distributions, and we compare our data to the models. We demonstrate that the IF model fails to fit the distribution of particles at large angles with respect to the jet axes, whereas the Lund SF model yields good agreement. We show that the Webber CF model, while untuned, provides a good description of the ratios of the particle populations between jets. In section 4 we compare the overall fits of the SF and IF models and verify that the failure of the IF model is not a consequence of the particular scheme or of the way it is tuned. Section 5 contains a further discussion of CF models. Our summary and conclusions are presented in section 6.

2 *Fragmentation models*

2.1 *SF and IF models*

Our SF and IF model event samples are generated with the Lund Monte Carlo program Jetset V5.2 [12]. This program implements the full 2nd order QCD matrix elements, i.e. the generation of $q\overline{q}$, $q\overline{q}g$, $q\overline{q}gg$ and $qq\overline{q}\overline{q}$ states, including the interference between the 2nd order virtual and 1st order $q\overline{q}g$ diagrams. The 3 and 4-jet Born cross sections each diverge as the invariant mass between two partons approaches zero. The total cross section is finite, however, because these divergences are canceled by similar divergences (of opposite sign) from the virtual corrections to the 2 and 3-jet final states, respectively. For the Monte Carlo simulation, a cutoff in the parton-parton invariant mass is introduced in order to obtain individually finite 2, 3 and 4-jet cross sections. Thus 4-jet states containing a small mass parton system are merged with the 3-jet states, for example. Such a merger corresponds physically to the impossibility of distinguishing a single jet from a jet which has emitted a

soft or colinear gluon. We maintain the invariant mass cutoff $Y_{min} = (p_i + p_j)^2/s$ at the default value of $Y_{min} = 0.02$ (p_i and p_j are the 4-momenta of any two partons). With $\sqrt{s} = 29$ GeV this corresponds to a minimum parton-parton invariant mass of 4.10 GeV/c^2 (in practice the Y_{min} cutoff is somewhat more complicated due to the effect of finite quark masses).

For SF, we use the symmetric Lund model [2], in which the initial quark-antiquark pair is represented by a massless relativistic string, with the q and $\overline{q}$ as endpoints. Gluons appear as "kinks", or transverse excitations, along this string. For IF, we use the independent fragmentation section of the Lund Monte Carlo program [12]. In contrast to SF, the quarks and gluons of IF are dynamically isolated from each other. Because of this isolation, IF models intrinsically cannot conserve energy and momentum simultaneously. Therefore, for the IF model, various algorithms have been developed to impose energy-momentum conservation after an event has been generated. In one such scheme, an IF event is boosted in the direction of the overall momentum imbalance to the frame in which this momentum imbalance is zero; particle energies are then rescaled by a common factor to obtain energy conservation. In this process the relative energies of the partons are approximately preserved; the parton directions are systematically shifted, however. In another scheme, the longitudinal momenta of particles are adjusted separately within each jet in such a manner that the ratio of the adjusted to original parton momentum is the same for all partons. Parton directions are thereby preserved while their relative energies are changed. In addition to this conservation problem, IF does not provide a specific model for gluons. Therefore, for IF, the Monte Carlo package provides various options for the gluon modeling (as well as for the

energy-momentum conservation scheme). We initially choose an IF mode in which the gluon fragments like a quark and in which energy-momentum is conserved so as to maintain parton directions. This variant is essentially equivalent to the Hoyer model [4]. We henceforth refer to this model as IF_1. In section 4 we verify that our results are independent of this choice.

The hadronization of the parton systems occurs in the same manner for both the SF and IF models. First, primary hadrons are created through the production of $q\overline{q}$ (or $qq - \overline{qq}$) pairs in the color force field of the initial quark or gluon. Second, unstable primary hadrons are decayed. The longitudinal momentum distribution of primary hadrons (along the string direction for SF and the parton direction for IF) is governed by a fragmentation function $f(z) = exp(-bm_t^2/z)(1-z)^a/z$. Here z is the fraction of the remaining jet energy-momentum given to a hadron when it is formed, and m_t is its transverse mass. The parameters a and b are determined by comparison with data. The transverse momentum distribution of primary hadrons is determined by the transverse momentum q_t given to the quarks and antiquarks (or diquarks and antidiquarks) produced from the color fields. This quark transverse momentum distribution is a Gaussian of the form $exp(-q_t^2/\sigma_q^2)$.

We perform a multi-parameter fit of our SF and IF models to the data as a prelude to our study of the 3-jet particle distributions. This ensures that the models have the correct multiplicity, overall momentum structure and 3-jet rate. There are five main parameters which affect these: the fragmentation parameters a, b and σ_q, the fraction r of vector (vs. pseudoscalar) mesons amongst primary hadrons and the strong coupling constant α_S. Since a and b are strongly correlated we fix b at 0.60 which gives a good representation of our D^* spectrum. We maintain r at the

default values of .50 for light quark mesons and .75 for mesons containing charm or bottom quarks. We then simultaneously fit α_S, a and σ_q to the entire hadronic event sample.

The experimental distributions used for the fit include charged particles only: consistent results are found if photons are included. These distributions can be classified into three sets 1, 2 and 3 according to their sensitivity to the model parameters α_S, a and σ_q, respectively, and are listed in Table 1. Q_1 and Q_2 are the smallest and next smallest eigenvalue of the sphericity tensor; L_1 and L_2 are the thrust values along the minor and major thrust axes; $< p_{\perp in} >$ and $(p_i)_{\perp in}$ are the average momentum per event and the momentum per particle in the event plane, and perpendicular to the sphericity axis; $< p_{out} >$ and $(p_i)_{out}$ are the average momentum per event and the momentum per particle out of the event plane defined by the vectors associated with the two largest sphericity eigenvalues; $x_p = 2p_i/E_{c.m.}$ is the scaled particle momentum and $\Delta M^2_{jet}/E^2_{vis}$ is the difference in the squares of the jet masses for an event divided into hemispheres by the plane normal to the sphericity axis, normalized to the visible energy E_{vis}. By fitting to three distributions at a time, one from each set, we constrain all three parameters. This results in $5 \times 2 \times 4 = 40$ combinations of the distributions and therefore in 40 values for each parameter. These multiple values provide a consistency check and are used to estimate the systematic error.

The same distributions are generated using the Monte Carlo models. We express each bin of each Monte Carlo distribution as a 1st order Taylor expansion in the parameters:

$$M_i(\alpha_S, a, \sigma_q) = M_i^0 + \frac{\partial M_i}{\partial \alpha_S}(\alpha_S - \alpha_S{}^0) + \frac{\partial M_i}{\partial a}(a - a^0) + \frac{\partial M_i}{\partial \sigma_q}(\sigma_q - \sigma_q^0) \qquad (1)$$

The 0th order term M_i^0 is the value of the Monte Carlo distribution in bin i evaluated at an "expansion point" $\alpha_S{}^0$, a^0, σ_q^0, initially the default values. The derivatives are the slopes of M_i as each parameter is varied. The expansion point term includes full detector simulation. The event generator without detector simulation is used to calculate the derivatives. A χ^2 function is defined to measure the agreement between experiment and Monte Carlo:

$$\chi^2(\alpha_S, a, \sigma_q) = \sum_{j=1}^{3} \left(\sum_{bin\ i=1}^{n} \frac{(D_i - M_i(\alpha_S, a, \sigma_q))^2}{\sigma_{D_i}^2 + \sigma_{M_i}^2 + \sigma_{syst_i}^2} \right)_{Distribution \in Set j} \tag{2}$$

D_i and M_i are the values of the data and Monte Carlo in bin i after normalization to the same number of events. The sum over j chooses a distribution from each of the sets 1, 2 and 3. σ_{D_i} and σ_{M_i} are the statistical errors on D_i and M_i; typically $\sigma_{M_i} \approx \frac{1}{2}\sigma_{D_i}$. σ_{syst_i} is an estimated systematic error set equal to 5% of M_i. It is included so that high statistics bins do not inordinately dominate the fits over the low statistics tails. Combining (1) and (2), we approximate $\chi^2(\alpha_S, a, \sigma_q)$ by a quadratic form in parameter space, the extremum of which predicts the parameter values which minimize χ^2. We use the average values predicted by the 40 combinations of distributions as our next expansion point and recalculate the derivatives around this point to obtain new predictions for the parameters. This process is iterated until the results are stable. Note that the linear approximation becomes fully justified as the parameters converge to their best-fit values.

To test this procedure we generated Monte Carlo data at several values of α_S, a and σ_q. Applying our procedure to these toy data samples we verified that the predictions always converged to the correct parameter values.

For our SF model we find $\alpha_S = .183 \pm .010$, $\sigma_q = .350 \pm .016$, $a = .955 \pm .100$ and for our IF_1 model $\alpha_S = .125 \pm .013$, $\sigma_q = .390 \pm .018$, $a = 1.23 \pm .12$. The errors include

both statistical and systematic contributions. The systematic error is estimated from the rms spread in the predictions of the 40 combinations of distributions. Figure 2 shows these predictions in the α_S, σ_q plane for our SF and IF_1 models. Both of these tuned models yield reasonably good fits to the experimental distributions of sets 1, 2 and 3: details will be discussed in section 4. In addition, both models provide good descriptions of our flavor identified cross sections, including those for charged pions, kaons and protons [10], K_s^0 and K^{*0} [13], Λ [14] and ϕ [15] particles.

2.2 *CF model*

Among the available CF models, we choose to concentrate on the Webber Monte Carlo [6]. This model is based on a parton shower generated using the leading-log approximation of QCD, extended to include the leading interference effects of soft gluons. In such a procedure the initial q or $\overline{q}$ evolves through multiple gluon bremsstrahlung, at each branch coming nearer its mass shell. Emitted gluons further branch through the processes $g \rightarrow gg$ and $g \rightarrow q\overline{q}$. Leading interference effects are accounted for by ordering the opening angles of parton emission such that each successive angle is smaller than the preceeding one [16]. This ordering is imposed throughout the event, beginning with the initial splitting $\gamma^* \rightarrow q\overline{q}$. The shower is continued until the virtual mass of each parton approaches the relevant quark mass, if the parton is a quark, or a cutoff Q_0, if it is a gluon, at which point remaining gluons decay into $q\overline{q}$ pairs. The color flow in an event associates each quark with a unique antiquark of opposite color, thus forming a system of color-singlet clusters. The mass of a cluster is given by the sum of the 4-momenta of its constituent q and $\overline{q}$; if this mass exceeds a threshold $M_{clust.}^{max}$, the cluster is split by $q\overline{q}$ production along the color string connecting them. In Version 1.1 of

the Monte Carlo used for our analysis, c and b quarks undergo β decay before the final clusters are formed. Therefore the clusters produced by the model contain u, d and s quarks only. These final-state clusters decay into 2-hadron states. The hadron spectrum is taken from the 0^{-+}, 1^{--}, 1^{++} and 2^{++} meson nonets and the $\frac{1}{2}^{+}$ and $\frac{3}{2}^{+}$ baryon multiplets with a probability determined by the 2-body phase space and the spin multiplicity. The dynamical suppression of baryons and particles with strange quarks is accomplished through the decreased phase space available for these hadrons because of their larger masses.

The main parameters of the Webber CF model are the QCD scale parameter Λ_{QCD}, the gluon mass cutoff Q_0, the maximum cluster mass $M_{clust.}^{max}$ and the masses of the u, d and s quarks. The shower development and cluster mass spectrum are primarily governed by the first three parameters, which for our Monte Carlo sample were maintained at the default values of Λ_{QCD} = 0.30 GeV, Q_0 = 0.70 GeV and $M_{clust.}^{max}$ = 3.5 GeV. The quark mass values were .34, .34 and .50 GeV for the u, d and s quarks, respectively. We do not apply our multi-parameter fit procedure to the Webber Monte Carlo as it lacks the exact 3-jet matrix elements, thus preventing a reasonable description of many distributions used in section 2.1 for the fit. Since the 3-jet analysis described in section 3 selects events with an approximately fixed momentum structure, however, this does not greatly affect the comparison of particle distributions made with the 3-jet sample. In section 5 we discuss the sensitivity of the Webber model predictions to the parameters of the model.

The Webber model predicts the correct multiplicity for charged pions, kaons and protons and yields a good fit of our inclusive charged pion and proton spectra. The

predicted inclusive charged kaon spectrum is too peaked at low momenta, however, due to the simplified treatment of heavy quark hadron decays.

3 *3-Jet event selection and particle distributions*

The 3-jet event selection is performed using both charged particles and photons. To identify a 3-jet sample, we first calculate the sphericity eigenvalues Q_1, Q_2 and Q_3 and associated eigenvectors $\vec{q}_1$, $\vec{q}_2$ and $\vec{q}_3$, defined such that $Q_1 < Q_2 < Q_3$ and $Q_1 + Q_2 + Q_3 = 1$. Preliminary 3-jet event candidates are selected by the cuts $Q_1 < .06$ and $Q_2 - Q_1 > .05$. Events for which the angle between $\vec{q}_3$ and the beam axis is smaller than 40 degrees are next rejected, as are events which have a total momentum imbalance $\mid \sum \vec{p}_i \mid / \sum \mid \vec{p}_i \mid$ greater than .40. These last two cuts are to eliminate events with jets or portions of jets outside the detector acceptance. Surviving events are subjected to a jet-finding algorithm (described below) which searches for 3-jet structure after projecting the particle momenta into the event plane defined by $\vec{q}_2$ and $\vec{q}_3$. The 3-jet event candidates are required to have at least 2 particles and 1.5 GeV of particle momentum in each jet. Our final sample consists of 3022 3-jet events, with an estimated background of about 20% from 2-jet and 4-jet events. Jet directions are given by the vector sum of the particle momenta which comprise the jet, after projection into the event plane. The jets are labelled 1, 2 and 3 according to the angles between them such that jet 1 is opposite the smallest angle and jet 3 is opposite the largest angle. Using the SF or IF_1 models, we estimate that jet 1, 2 and 3 is the gluon jet in 7, 18 and 55% of the events, respectively.

Our jet-finder is based on thrust cuts in the following manner [17]. We initially

assume a large number of jets in an event, $N_{jet} = N_0 \approx 8$, defined by the highest momentum particles and the low momentum particles near to them in angle. The generalized thrust

$$T_{N_0} = \sum_{k=1}^{N_0} \left| \sum_{i \in S_k} \vec{p_i} \right| \Big/ \sum_{i=1}^{N_p} |\vec{p_i}|$$

is calculated, with N_p the total number of particles and S_k the set of particles assigned to the kth jet. Initially, with N_0 large, $T_{N_0} \approx 1$. The two jets closest in angle are then merged to form an $N_{jet} = N_0 - 1$ jet configuration. Particles are reassigned to the nearest jet, in angle, and the jet axes recalculated. This process is repeated until the particle assignments are stable. The generalized thrust T_{N_0-1} and the ratio $R_{N_0} = T_{N_0}/T_{N_0-1}$ are calculated. If $R_{N_0} \geq 1.05$ the original jet configuration with N_0 jets is accepted, otherwise the two nearest jets are again merged and particles reassigned, forming an $N_{jet} = N_0 - 2$ jet configuration. This process is continued until $R_{N_{jet}} \geq 1.05$; when this occurs, the N_{jet} configuration is accepted as the correct jet assignment for the event.

The angular distribution of particles in the 3-jet sample, $(1/N)\, dN/d\phi$, is presented in Figure 3. ϕ is the angle in the event plane between the direction of a particle and jet 1. Also shown are the predictions of the SF, IF_1 and CF models of section 2. The distributions are normalized to the total number of particles in each sample. ϕ proceeds from jet 1 at $\phi = 0^o$ through jet 2 ($\phi \approx 155^o$) to jet 3 ($\phi \approx 230^o$) back to jet 1 ($\phi = 360^o$). The statistical errors of all model curves are approximately half those shown for the data points.

Figure 3(a) shows $(1/N)\, dN/d\phi$ for all charged particles and photons. The SF model provides a good description of the data over the entire ϕ range. The IF_1 model provides nearly as good a description of the jet peaks and of the regions

between jets 2 and 3 and between jets 1 and 3: the particle density of the jet 1-2 region is over-predicted, however, by about 30%. The untuned CF model also reproduces the jet peaks, but over-predicts the particle density in all the regions between jets. As a measure of the goodness-of-fit to the jet 1-2 region, we calculate χ^2 for the interval $40^o < \phi < 120^o$. For the 16 bins of this interval, χ^2= 11.8, 79.6 and 57.9 for the SF, IF_1 and CF models, respectively.

Figures 3(b) and 3(c) show $(1/N)\ dN/d\phi$ for charged particles and photons satisfying $0.3 < p_{out} < 0.5$ GeV and for a heavy particle sample (with about 80% purity) of charged kaons and protons [10], neutral kaons [13] and lambdas [14]. Particles with p_{out} larger than 0.5 GeV are excluded from Figure 3(b) because these particles are more difficult to associate with a particular jet 1, 2 or 3 and thus obscure the jet structure of the event. The neutral kaons and lambdas of Figure 3(c) are reconstructed geometrically through a search for secondary vertices, while the charged kaons and protons are identified with a weighted χ^2 technique based on simultaneous dE/dx and momentum measurements (see Ref.[15] for a description). Only those protons not used in the lambda reconstruction are included. With the exception of the region between jets 1 and 2, the SF and IF_1 models are again in reasonable agreement with the data and with each other. In the jet 1-2 region, however, the discrepancy of the IF_1 model with the data is enhanced over that in Figure 3(a) (the particle density is over-predicted by a factor of 2 in both Figures 3(b) and 3(c)), while the SF model provides a good description. As before, the untuned CF model over-predicts the particle density between all jets. For the 8 bins in the interval $40^o < \phi < 120^o$, the SF, IF_1 and CF models provide χ^2's of 12.5, 43.2 and 11.5 for the distribution of Figure 3(b), and χ^2's of 12.5, 48.6 and

36.1 for the distribution of Figure 3(c), respectively.

The depletion of particles in the $q\overline{q}$ region of the SF model occurs because the qg and $\overline{q}g$ string segments (Figure 1(a)) each fragment in their own rest frame: thus the hadron sources (i.e., strings) are Lorentz-boosted relative to the overall event center-of-mass. Particles are distributed symmetrically around the string segments in the fragmentation rest frames. In the overall center-of-mass, the component of each particle momentum $\vec{p}_i$ along the direction of the boost $\hat{n}_B$ becomes $\vec{p}_i \cdot \hat{n}_B \rightarrow \gamma_B(\vec{p}_i \cdot \hat{n}_B + \beta_B E_i)$, where β_B and γ_B are the boost parameters. Momentum components perpendicular to $\hat{n}_B$ are unchanged. $\hat{n}_B$ points away from the $q\overline{q}$ region for both string segments. Thus the particle distribution becomes asymmetric, with more particles on the side of the string opposite the $q\overline{q}$ region. This "depletion effect", or "boost signal", is enhanced as $E_i/(\vec{p}_i \cdot \hat{n}_B)$ increases, e.g. for particles with a large energy compared to momentum along the boost direction. Therefore the relative depletion of particles in the $q\overline{q}$ region is greater for particles with large mass or large p_{out}, the momentum component of a particle out of the event plane. We note that an observable depletion signal also depends upon the limited transverse momentum available to hadrons in the SF model, since this prevents particles from crossing over into the $q\overline{q}$ region.

As a measure of the relative depletion we calculate the normalized particle population between jets, $\mathcal{N}_{ij}$, defined as follows. For each particle between jets i and j, after projection into the event plane, we divide the angle between jet i and the particle by the angle between jets i and j. This normalizes each particle angle to be between 0 (along jet i) and 1 (along jet j). $\mathcal{N}_{ij}$ is the number of particles in this normalized angle region from .3 to .7. Since the particles in this region are soft

and between jets, they are those which are most susceptible to boost effects. The particle population in the $q\overline{q}$ region relative to the qg (or $\overline{q}g$) region can then be expressed quantitatively in terms of the ratio $\mathcal{N}_{31}/\mathcal{N}_{12}$. In forming such a ratio, we anticipate that details of the acceptance, normalization and transverse momentum distribution modeling between jets will cancel. This is explicitly verified in section 4. We also expect that the lack of tuning for the CF model should be less relevant for this ratio. This question is examined in section 5.

For IF models, the regions between jets are dynamically equivalent and one expects $\mathcal{N}_{31}/\mathcal{N}_{12} \sim 1$. Furthermore $\mathcal{N}_{31}/\mathcal{N}_{12}$ should demonstrate no p_{out} or mass dependence in IF models. In contrast, this ratio should be greater than 1 for models demonstrating a boost signal, and increase in magnitude as p_{out} or mass increases.

The ratio $\mathcal{N}_{31}/\mathcal{N}_{12}$ is displayed in Figure 4. Figures 4(a) and 4(b) show $\mathcal{N}_{31}/\mathcal{N}_{12}$ for dE/dx identified pions in two p_{out} intervals. We select a single particle type for these figures (i.e. charged pions) in order to distinguish the p_{out} dependence from the mass dependence. This is necessary because particle fractions also vary with p_{out} [18]. Figures 4(c) and 4(d) show $\mathcal{N}_{31}/\mathcal{N}_{12}$ for all charged pions and for the heavy particles of Figure 3(c). The data demonstrates that $\mathcal{N}_{31}/\mathcal{N}_{12}$ is significantly greater than 1. In addition, $\mathcal{N}_{31}/\mathcal{N}_{12}$ is enhanced for pions with large p_{out} (Figure 4(b), $0.3 < p_{out} < 0.5$ GeV) relative to pions with small p_{out} (Figure 4(a), $0.0 < p_{out} < 0.2$ GeV). As mass is increased (Figures 4(c) and 4(d)), $\mathcal{N}_{31}/\mathcal{N}_{12}$ shows a similar enhancement. The SF model is in good agreement with the data both as to the magnitude of the effect and as to the mass and p_{out} behavior. The CF model also correctly predicts these effects. However, $\mathcal{N}_{31}/\mathcal{N}_{12}$ is approximately 1 for the IF_1 model in Figures 4(a)-4(d) and exhibits no mass or p_{out} dependence, as expected.

Thus the predictions of the IF_1 model are in direct contradiction with the data.

As a further test of this depletion signal, we eliminate those events for which jets 2 and 3 are nearly degenerate in energy, in order to increase the probability that jet 3 is the gluon jet. By requiring the ratio $(E_{Jet2} - E_{Jet3})/E_{Jet3}$ to be greater than 0.20, the probability that jet 3 is the gluon jet is increased to 58% (while the 3-jet sample is reduced to 2528 events). Table 2 displays the values of $\mathcal{N}_{31}/\mathcal{N}_{12}$ both with and without this additional event cut. As seen from the table, the level of $\mathcal{N}_{31}/\mathcal{N}_{12}$ increases for all categories as the probability that jet 3 is the gluon jet is raised. This increase is also present for the SF and CF models; no dependence on this probability is observed for the IF_1 model, however.

4 *Comparison of overall SF and IF model predictions*

In this section we present a quantitative study of the overall SF and IF model fits, including a comparison of the goodness-of-fit for distributions using the entire hadronic event sample to that for the 3-jet heavy particle distribution. We verify that the discrepancies observed between the IF_1 model and the data in section 3 are not an artifact of the particular IF model chosen by studying IF models with different gluon or momentum conservation schemes. In addition, we test the sensitivity of the model predictions on the parameters.

The additional IF event generator routines are all provided by the Lund Monte Carlo package Jetset V5.2 [12]. The particular choices are listed in Table 3. The parameters of each model are tuned using the multi-parameter fit technique of section 2.1, with this difference: in section 2.1 we compare uncorrected data to a Monte Carlo expansion point which includes detector simulation whereas here

we compare corrected data directly to the event generator. Both methods give consistent results for the SF and IF_1 models of sections 2 and 3. Table 3 summarizes the results of our fits for all SF and IF models. Note the strong model dependence of the parameter α_S.

To perform the comparison of the overall fits, we display in Table 4 the per cent differences per bin between the corrected data and optimized models for the distributions of sets 1, 2 and 3 (c.f. Table 1) and for the 3-jet heavy particle distribution $(1/N)\, dN/d\phi$ with $40^o < \phi < 120^o$. We choose this latter distribution because it exhibits a large discrepancy with the IF_1 model (Figure 3(c)) and we wish to study this discrepancy in a systematic manner. The values of Table 4 are calculated by averaging the quantity $100 \cdot (D_i - M_i)/D_i$ over each distribution, where D_i and M_i are the values of the data and model, respectively, in bin i of the distribution. We quote mean per cent differences rather than χ^2's so as to compare the goodness-of-fit of histograms based on the entire hadronic sample to those based on the much smaller 3-jet sample. This method is more sensitive to systematic differences in bins with small statistics, e.g. the tails of distributions. In calculating the values of Table 4, each distribution is normalized by the number of events in the total hadronic event sample, except for the $(1/N)\, dN/d\phi$ distribution which is normalized by the number of particles as in Figure 3. All conclusions are unchanged if, for example, we normalize the 3-jet particle distribution by the number of 3-jet events.

First we consider the global event distributions of sets 1, 2 and 3. The SF distribution with the worst fit is the Q_1 distribution, with a mean difference of 21.3%, shown in Figure 5. For the IF models, the worst fit occurs for the $\Delta M^2/E^2_{vis}$

distribution, e.g. a mean difference of -24.8% for the IF_1 model (Figure 6). In general, however, the distributions of set 3 have the worst fits for all models, i.e. Q_1 or $< p_{out} >$ provides the 2nd or 3rd largest discrepancy in all cases. Thus a general problem of the SF and IF models is a description of the distributions involving the momentum component out of the event plane.

To study this problem, we compared the jet multiplicity of the data to that predicted by the SF and IF_1 models. Using our jet-finder (see section 3) to count the number of jets, we find that the predicted 4-jet rate is too small in both models. Correspondingly, the 3-jet rate is too high because the multi-parameter fit compensates for the 4-jet deficiency through an increased value for α_S. To simulate this missing 4-jet structure, we generated additional 4 parton events with a minimum parton-parton invariant mass of 7 GeV. By choosing the number of such events so that they comprise 1% of each Monte Carlo sample, and then refitting the models, the agreement of the models with the jet multiplicity in the data is improved. The shapes of the Q_1 and $\Delta M^2/E^2_{vis}$ distributions for these 4-parton events are displayed in Figures 5 and 6 by the dashed curves, for the SF and IF_1 models, respectively (the ordinate for these curves is in arbitrary units). Mean differences for these refit models are shown by the numbers in parentheses in the SF and IF_1 columns of Table 4. The fits to the distributions of set 3 show uniform improvement, for both models. In addition, the fit of the IF_1 model to the $\Delta M^2/E^2_{vis}$ distribution is improved. Thus the discrepancies of these models with the data are generally of similar nature and magnitude and the tuned SF and IF models provide equally good descriptions for the distributions of sets 1, 2 and 3.

In contrast, there is a wide disparity between the SF and IF models in the fit

of the heavy particle $(1/N)\, dN/d\phi$ distribution with $40^o < \phi < 120^o$. The mean difference from the measured distribution is -9.9% for the SF model but -56.4%, or greater, for all IF models. This demonstrates the insensitivity of the jet 1-2 region to the details of the gluon or momentum conservation modeling. Including the additional 4-jet events raises these mean differences to -12.8% for SF and to -65.0% for IF_1, thus preserving the relative disparity between models. These latter differences correspond to χ^2's of 5.3 and 37.7, respectively, for the 8 bins of the region $40^o < \phi < 120^o$: thus the SF model still provides a good description of the data (the χ^2's are smaller here than in section 3 because of the larger errors associated with the corrected data).

To show that the IF model cannot be tuned to agree with the data, we tune the parameters of the IF model to give the best possible fit of the jet 1-2 region. Thus we apply our multi-parameter fit technique to the single heavy particle $(1/N)\, dN/d\phi$ distribution, with $40^o < \phi < 120^o$. We use the IF_1 model, in which the gluon fragments as a quark and in which energy-momentum is conserved so as to preserve the parton directions. This single distribution converges to the parameter values $\alpha_S = .120 \pm .024$, $\sigma_q = .120 \pm .055$, $a = 0.75 \pm 0.18$, where the errors are statistical only. The mean per cent differences for this model, labeled IF_1', are shown in the last column of Table 4. Although the fit to the jet 1-2 region of the 3-jet heavy particle distribution is improved, the overall fit of the other histograms is worsened. In fact the maximum discrepancy for the IF_1' model, shown in the last row of Table 4, is 54.9%, virtually as large as the maximum discrepancy for all the other IF models. We conclude that the IF model, in contrast to the SF model, cannot simultaneously fit all distributions. In particular the IF model cannot be tuned to agree with the

data in the jet 1-2 region of the heavy particle $(1/N)\ dN/d\phi$ distribution with a reasonable set of parameter values.

Table 5 lists the ratio $\mathcal{N}_{31}/\mathcal{N}_{12}$ for the four particle categories of Figures 4(a)-4(d), again using the SF and IF models at the event generator level. The IF models are in general agreement with each other. None of them predicts a significant increase in $\mathcal{N}_{31}/\mathcal{N}_{12}$ as p_{out} for the pions or as particle mass is increased. The values of Table 5, which contain no detector simulation, are consistent with those found for the SF and IF_1 models using full detector simulation (Table 2), demonstrating that $\mathcal{N}_{31}/\mathcal{N}_{12}$ is independent of acceptance factors. Similarly, the agreement of the IF_1 and IF_5 model predictions, for example, shows that this ratio is insensitive to details of the transverse momentum distribution modeling.

Our conclusion is that the failure of the IF model to describe the absolute 3-jet particle density or to reproduce the p_{out} and mass dependences observed in the data is not an artifact of a particular scheme or of the tuning of the parameters but is a fundamental characteristic of the model.

5 *Discussion of CF model*

The Webber CF model generally over-predicts the particle density between jets, as observed in Figures 3(a) and 3(b). However, the model provides a good description of the ratio of those densities, as seen in Figures 4(a)-4(d). To study the sensitivity of the predictions to the parameters of the model, we varied Q_0 and $M_{clust.}^{max}$ and observed the effect upon these distributions. The parameter Λ_{QCD} was not varied because its value primarily determines the number of 3-jet events and not the event shape. The quark masses were not changed because they are deter-

mined by considerations external to the model. We find that the particle density distributions of Figure 3 are especially sensitive to $M_{clust.}^{max}$. By lowering $M_{clust.}^{max}$ to 2.8 GeV, for example, we markedly improve the description of the regions between jets, while the ratio $\mathcal{N}_{31}/\mathcal{N}_{12}$ is only slightly affected. This reduction in $M_{clust.}^{max}$ destroys the agreement of the model with our measured proton multiplicity. However, preliminary studies indicate the possibility of restoring this agreement by including heavy quark hadron decays. Therefore we feel that the disagreement of the Webber model with the distributions of Figure 3 is not fundamental and that it may be remedied by future improvements. On the other hand, the relative insensitivity of $\mathcal{N}_{31}/\mathcal{N}_{12}$ to reasonable variations of the parameters indicates that it is a good quantity to use in testing the predictions of the model.

In contrast to the Lund SF case, the physical mechanism responsible for the depletion effect in the Webber CF model is not obvious. Thus it is not clear whether the effect arises from an intrinsic property of the the parton shower, as a consequence of the color flow (i.e., the way partons are combined to form the color-singlet clusters) or because high mass clusters (those above the $M_{clust.}^{max}$ threshold) decay like a string. We therefore calculated $\mathcal{N}_{31}/\mathcal{N}_{12}$ at the parton shower, cluster and hadron levels to determine the source of the effect in the Webber model. By "parton shower level", we mean the distribution of quarks and gluons at the end of the perturbative shower, before cluster formation; by "cluster level", we mean the distribution of those clusters which decay into hadrons. For these calculations, the event samples were identified by applying the 3-jet event selection of section 3 to either the parton, cluster or hadron distributions (except without a minimum multiplicity requirement on each of the three jets). Both quark-antiquark and

gluon-gluon events were generated, leading to $q\bar{q}g$ and ggg 3-jet Webber model samples, respectively. This latter sample allows us to determine the importance of the event color flow in producing the observed depletion. Figures 7(a) and 7(b) show schematic representations of an event from each of these two samples.

To provide a contrast for the Webber model, we calculated $\mathcal{N}_{31}/\mathcal{N}_{12}$ for the Gottschalk CF model [7] as well. The Gottschalk model, like the Webber model, is based on a perturbative shower generated using the leading-log approximation of QCD. However, the Gottschalk parton shower does not include the effects of soft gluon interference so that the parton emission angles are not ordered. We also studied that subset of Gottschalk events for which the ordering of emission angles is coincidentally satisfied (about 18% of the events). The average Gottschalk model cluster mass is larger ($\sim$ 4 GeV) than that of the Webber model ($\sim$ 1 GeV); these high mass clusters evolve, through a string breaking mechanism, into softer clusters which in turn decay to hadrons (according to a parameterization of low energy data). Our version of the Gottschalk CF model is dated March 28, 1984. The principal parameters have the values $\Lambda_{QCD} = 0.62$ GeV, $t_c = 15.0\, GeV^2$, $W_{min} = 1.75$ GeV, $W_{max} = 4.0$ GeV, $W_c = 0.5$ GeV and $\rho_c = 2.50\, GeV^{-2}$, in the formalism of Ref. [7].

Our results are listed in Table 6. At the parton shower level, $\mathcal{N}_{31}/\mathcal{N}_{12} = 1.33 \pm .05\,(1.30 \pm .06)$ for the Webber $q\bar{q}g$ (ggg) sample, while $\mathcal{N}_{31}/\mathcal{N}_{12} = 1.00 \pm .05$ $(1.12 \pm .05)$ for the standard (ordered) Gottschalk sample. Both the Webber $q\bar{q}g$ and ggg initiated showers therefore demonstrate a depletion of partons in the jet 1-2 region, relative to the jet 1-3 region. This depletion is not related to the color flow in an event since it has the same magnitude in both cases. The partons of the ordered Gottschalk shower also exhibit a significant jet 1-2 depletion, while those

of the standard Gottschalk shower do not. We conclude that the depletion effect of the Webber model, at the parton level, is a direct consequence of the angular ordering constraint. This ordering forces the parton shower of the Webber model into forward directions along the jet axes, unlike the shower in the standard Gottschalk events. The Webber $q\overline{q}g$ or ggg initiated shower is therefore less likely to populate the central jet 1-2 region (relative to the 1-3 or 2-3 regions) because this region corresponds to the largest angle between jets: the central section of this region is thus the furthest, in angle, from the jet axes.

At the cluster level, the color structure of the Webber $q\overline{q}g$ vs. ggg events becomes relevant. For the $q\overline{q}g$ sample, clusters form between jets 1 and 3 and between jets 2 and 3, i.e. between the gluon and the quark or antiquark, to locally neutralize the color charges of the separating partons. Since the q and $\overline{q}$ have but a single color index, no clusters form between jets 1 and 2 (Figure 7(a)). The result is an increase in the ratio $\mathcal{N}_{31}/\mathcal{N}_{12}$ from the parton level value of $1.33 \pm .05$ to $1.82 \pm .08$. This increase is also observed for the clusters of the ordered Gottschalk events (Table 6). For ggg events, clusters form in all the regions between jets. In particular they form between jets 1 and 2 to neutralize the second color indices of those gluon jets (Figure 7(b)). The clusters between jets 1 and 2 are, on average, of higher mass than those in other regions and are more likely to split, further increasing the cluster multiplicity of that region. Thus the ratio $\mathcal{N}_{31}/\mathcal{N}_{12}$ is reduced from its parton shower value of $1.30 \pm .06$ to $1.16 \pm .04$. Therefore the specific color structure of a $q\overline{q}g$ event is required to preserve the depletion signal at this level.

At the hadron level, the depletion effect is partly washed out by the phase space decays of the clusters. The overall behavior is preserved, however, because

the limited momentum available to hadrons from the low cluster-mass spectrum prevents particles from crossing into the $q\overline{q}$ region (a similar mechanism limits the transverse momentum of hadrons in the Gottschalk model). Thus the hadrons in Webber (and ordered Gottschalk) $q\overline{q}g$ events demonstrate a jet 1-2 depletion ($\mathcal{N}_{31}/\mathcal{N}_{12}$= 1.33 ± .04); however, there is no significant depletion observable for the hadrons produced in Webber ggg events ($\mathcal{N}_{31}/\mathcal{N}_{12}$= 1.07 ± .02). We have verified that the enhancement of the depletion signal with increased hadron mass or p_{out} occurs because such particles have a smaller Q-value in the plane of the event and thus more closely follow the cluster directions in that plane, as observed from the overall center-of-mass. In this sense, the depletion effect of the Webber model is a "boost signal" in the same sense as discussed for the SF model in section 3; i.e., the hadron depletion – including the mass and p_{out} enhancements – is a consequence of the motion of the hadron sources (in this case, clusters) away from the jet 1-2 region. We note in passing that the hadrons produced in ggg events generated with the Lund model "onia" decay routine [12] at $\sqrt{s}$ = 29 GeV do not exhibit a significant depletion signal ($\mathcal{N}_{31}/\mathcal{N}_{12}$ = 1.08 ± .02 for these hadrons, consistent with the corresponding value shown in Table 6 for Webber ggg events). Thus the Lund model also requires a color gap between the q and $\overline{q}$ in order to exhibit a jet 1-2 depletion.

6 *Summary and conclusions*

The three fragmentation models SF, IF and CF have been tested using their predictions for the distributions of particles between jets in 3-jet events. Our principal conclusion is that the IF model fails to describe the data. This failure is not

only an inability to explain the depletion of particles between jets 1 and 2, but a contradiction with the data as to the dynamical behavior of that depletion as particle mass or momentum out of the plane (or the probability that jet 3 is the gluon jet) is varied. The IF and SF models are identical at the perturbative level, in their predicted spectra of hadron resonances and in their particle branching ratios. They are equally well tuned to describe the event multiplicity and momentum distributions based on the entire data sample. Furthermore, the predictions of the IF model are largely independent of the particular gluon or momentum conservation scheme, the detector acceptance and the transverse momentum distribution modeling. Therefore we believe that the failure of IF – and the success of SF – in describing the data can be attributed to the representation of the non-perturbative dynamics, and that the failure of the IF model is indeed fundamental.

The Webber CF model also provides a good description of the relative particle depopulation in the jet 1-2 region: thus the correct prediction of the depletion effect is not limited to SF models. As discussed in section 5, this success is mainly a consequence of the ordering of partonic emission angles, of the event geometry and color structure, and of kinematical constraints imposed by the cluster mass scale. It is to be hoped that future improvements to the Webber model – not affecting these features – will allow a better prediction of the absolute particle density, $(1/N)\, dN/d\phi$. A modified Gottschalk CF model which includes the effects of soft gluon interference could presumably also provide a good description of the data.

To generalize, then, both the SF and CF models successfully predict the jet 1-2 depletion effect because of three features. First, both models implement mechanisms

early in the event history to suppress particle production between the q and $\overline{q}$. In SF this asymmetry is a consequence of the nature of the gluon as a kink on a string connecting the q and $\overline{q}$; in CF it is a consequence of the soft gluon interference. Second, the color screening connects the gluon jet to the quark and antiquark jets, in both models, leaving a gap in the color flow between the q and $\overline{q}$ (for SF the kink nature of the gluon is responsible for this as well). Third, the limited transverse momenta of hadrons prevents fragmentation products from randomly filling the regions between jets, thereby preserving the underlying structure. A more global conclusion might be that models displaying azimuthal symmetry around the jet axes cannot describe the data, while our results provide evidence that the sources of hadrons in e^+e^- annihilation are Lorentz-boosted relative to the overall center-of-mass. The effect can be considered a null result – a lack of particles – requiring the presence of all three features listed above, thus emphasizing the sensitivity of the particle populations between jets as a test of fragmentation models.

We acknowledge the efforts of the PEP staff, and the engineers, programmers and technicians of the collaborating institutions who made this work possible. This work was supported by the Department of Energy under contracts DE-AC03-76SF00098, DE-AM03-76SF00034, and DE-AC02-76ER03330, the National Science Foundation and the Joint Japan-US Collaboration Program in High Energy Physics. We would also like to thank Bryan Webber for helpful discussions about his model.

References

[1] See, for example, E. Reya, Phys. Rep. 69, 195 (1981); A.H. Mueller, Phys. Rep. 73, 237 (1981); G. Altarelli, Phys. Rep. 81, 1 (1981).

[2] B. Andersson,G. Gustafson,B. Söderberg, Z. Phys. C20, 317 (1983).

[3] A. Ali et al., Phys. Lett. B93, 155 (1980).

[4] P. Hoyer et al., Nucl. Phys. B161, 349 (1979).

[5] G.C. Fox and S. Wolfram, Nucl. Phys. B168, 285 (1980); R.D. Field and S. Wolfram, Nucl. Phys. B213, 65 (1983).

[6] B.R. Webber, Nucl. Phys. B238, 492 (1984).

[7] T.D. Gottschalk, Nucl. Phys. B214, 201 (1983); B239, 325 (1984); B239, 349 (1984).

[8] JADE Collab., W. Bartel et al., Phys. Lett. B134, 275 (1984).

[9] TPC Collab., H. Aihara et al., IEEE Trans. Nucl. Sci. 30, 63, 76 (1983).

[10] TPC Collab., H. Aihara et al., Phys. Rev. Lett. 52, 577 (1984).

[11] TPC Collab., H. Aihara et al., IEEE Trans. Nucl. Sci. 30, 117 (1983); H. Aihara et al., Nucl. Instr. and Meth. 217, 259 (1983).

[12] T. Sjöstrand, Comput. Phys. Commun. 27, 243 (1982); 28, 229 (1983).

[13] TPC Collab., H. Aihara et al. LBL-18325 (1984), to be published.

[14] TPC Collab., H. Aihara et al. LBL-18382 (1984), to be published.

[15] TPC Collab., H. Aihara et al., Phys. Rev. Lett. 52, 2201 (1984).

[16] A.H. Mueller, Phys. Lett. 104B, 161 (1981); Yu.L. Dokshitzer et. al., Phys. Lett. 115B, 242 (1982); L.V. Gribov et. al., Phys. Rep. 100, 1 (1983); A. Bassetto et. al., Phys. Rep. 100, 201 (1983).

[17] See A. Bäcker, Z. Phys. C12, 161 (1982).

[18] TPC Collab., H. Aihara et al., Phys. Rev. Lett. 53, 130 (1984).

Table Captions

Table 1. Experimental distributions used for the multi-parameter fit of the SF and IF_1 models.

Table 2. N_{31}/N_{12} for data and for models with full detector simulation. The numbers in parentheses indicate an event sample in which the probability that jet 3 is the gluon jet has been increased (see text).

Table 3. Optimum parameter values for SF and IF models. IF_1, IF_2 and IF_5 fragment the gluon as a quark. For IF_5 the Gaussian width of the gluon (σ_g), relative to that of the quark (σ_q), is included in the fit. IF_3 fragments the gluon as a $q\overline{q}$ pair with momentum shared according to the Altarelli-Parisi splitting function. IF_4 uses a Lund gluon, in which a q and $\overline{q}$ share momentum equally. D and E refer to the energy-momentum conservation scheme: for D the parton directions are preserved, for E the parton energies are preserved. The errors include statistical and systematic contributions. The longitudinal fragmentation parameter b is 0.60 for all models.

Table 4. Mean per cent difference per bin between distributions of the optimized SF and IF models at the event generator level and the corrected data. Model IF_1' is the same as IF_1 except the parameter values have been tuned to give the best possible fit of the heavy particle $(1/N)\, dN/d\phi$ distribution in the interval $40^o < \phi < 120^o$. The numbers in parentheses in the SF and IF_1 columns refer to fits of those models for which additional 4-parton events with a minimum parton-parton mass of 7 GeV have been included.

Table 5. $\mathcal{N}_{31}/\mathcal{N}_{12}$ for SF and IF models, at the event generator level.

Table 6. $\mathcal{N}_{31}/\mathcal{N}_{12}$ for Webber and Gottschalk CF models, at the event generator level.

Table 1 .

Set 1 "α_S"	Set 2 "a"	Set 3 "σ_q"
Q_2	x_p	Q_1
L_2	Charged Multiplicity	L_1
$< p_{\perp in} >$		$< p_{out} >$
$(p_i)_{\perp in}$		$(p_i)_{out}$
$\Delta M^2_{jet}/E^2_{vis}$		

Table 2.

Particle Sample	IF_1 Model	SF Model	CF Model	Data
All Charged & Photons	$0.99 \pm .02$ $(0.99 \pm .02)$	$1.24 \pm .03$ $(1.28 \pm .03)$	$1.25 \pm .03$ $(1.31 \pm .03)$	$1.19 \pm .05$ $(1.24 \pm .06)$
$\pi^{\pm}$ $0.0 < p_{out} < 0.2$ GeV	$0.98 \pm .03$ $(0.96 \pm .03)$	$1.11 \pm .04$ $(1.13 \pm .04)$	$1.16 \pm .03$ $(1.21 \pm .04)$	$1.13 \pm .07$ $(1.17 \pm .08)$
$\pi^{\pm}$ $0.3 < p_{out} < 0.5$ GeV	$0.98 \pm .07$ $(0.98 \pm .07)$	$1.28 \pm .09$ $(1.31 \pm .10)$	$1.31 \pm .09$ $(1.41 \pm .11)$	$1.67 \pm .24$ $(1.85 \pm .30)$
All $\pi^{\pm}$	$1.00 \pm .03$ $(0.98 \pm .03)$	$1.16 \pm .03$ $(1.19 \pm .03)$	$1.18 \pm .03$ $(1.24 \pm .03)$	$1.17 \pm .06$ $(1.23 \pm .07)$
Heavy Particles	$1.00 \pm .07$ $(1.02 \pm .08)$	$1.54 \pm .12$ $(1.77 \pm .16)$	$1.56 \pm .11$ $(1.56 \pm .13)$	$1.58 \pm .28$ $(1.59 \pm .30)$

Table 3.

Model	Model Description	α_S	σ_q	a	σ_g/σ_q
SF	Lund	$.183 \pm .010$	$.350 \pm .016$	$.955 \pm .100$	·
IF_1	$g = q, D$	$.125 \pm .013$	$.390 \pm .018$	1.23 ± 0.12	1.00
IF_2	$g = q, E$	$.147 \pm .015$	$.375 \pm .014$	1.10 ± 0.12	1.00
IF_3	$g = q\overline{q}, D$	$.120 \pm .011$	$.400 \pm .014$	1.20 ± 0.11	1.00
IF_4	$g = \text{Lund}, E$	$.160 \pm .027$	$.385 \pm .020$	$.830 \pm .260$	·
IF_5	$g = q, E$	$.135 \pm .015$	$.355 \pm .022$	1.23 ± 0.12	1.50 ± 0.37

Table 4.

Model		SF		IF_1		IF_2	IF_3	IF_4	IF_5	IF_1'
Set 1	Q_2	3.8	(0.9)	0.6	(4.5)	3.4	2.2	6.7	4.4	15.4
	L_2	3.2	(2.0)	−1.5	(1.0)	0.5	0.1	0.2	2.6	−21.6
	$< p_{\perp in} >$	−2.5	(−2.7)	−3.5	(3.4)	−5.1	3.2	6.3	−8.8	−10.5
	$(p_i)_\perp$	4.2	(2.8)	1.8	(6.5)	4.2	4.5	12.7	4.1	15.5
	$\Delta M^2_{jet}/E^2_{vis}$	−7.8	(−8.2)	−24.8	(−16.3)	−23.3	−20.8	−28.5	−21.7	−18.1
Set 2	x_p	5.5	(6.0)	2.9	(6.4)	0.1	0.2	−13.3	4.7	−10.9
	Chrgd.Mult.	5.6	(1.4)	1.3	(−1.6)	−1.8	−7.5	−18.5	5.3	−30.0
Set 3	Q_1	21.3	(13.6)	10.9	(4.1)	13.8	2.9	−2.6	12.2	54.9
	L_1	15.3	(10.3)	4.0	(0.3)	6.9	3.5	−4.2	3.8	30.7
	$< p_{out} >$	9.9	(7.6)	9.1	(8.2)	11.3	7.4	13.4	2.3	18.1
	$(p_i)_{out}$	7.3	(5.2)	5.1	(4.8)	4.4	4.0	4.1	3.1	43.0
Heavy Particle $(1/N)\, dN/d\phi$ $40^o < \phi < 120^o$		−9.9	(−12.8)	−59.4	(−65.0)	−56.4	−62.3	−63.3	−58.2	−16.3
Maximum Discrepancy		21.3	(13.6)	−59.4	(−65.0)	−56.4	−62.3	−63.3	−58.2	54.9

Table 5.

Particle Sample	SF Model	IF_1 Model	IF_2 Model	IF_3 Model	IF_4 Model	IF_5 Model	IF_1' Model
$\pi^{\pm}$ $0.0 < p_{out} < 0.2$ GeV	1.15 ± .02	1.00 ± .02	1.04 ± .02	1.01 ± .02	1.06 ± .02	0.97 ± .02	0.99 ± .02
$\pi^{\pm}$ $0.3 < p_{out} < 0.5$ GeV	1.42 ± .05	1.09 ± .04	1.09 ± .04	1.04 ± .04	1.11 ± .04	1.08 ± .04	1.04 ± .06
All $\pi^{\pm}$	1.21 ± .02	1.02 ± .01	1.05 ± .01	1.02 ± .01	1.08 ± .01	1.01 ± .01	1.01 ± .01
Heavy Particles	1.54 ± .05	1.03 ± .03	1.07 ± .03	1.06 ± .03	1.14 ± .03	1.03 ± .03	1.04 ± .03

Table 6.

Model	Webber $q\bar{q}g$	Webber ggg	Gottschalk (standard)	Gottschalk (ordered)
Parton Shower	$1.33 \pm .05$	$1.30 \pm .06$	$1.00 \pm .05$	$1.12 \pm .05$
Clusters	$1.82 \pm .08$	$1.16 \pm .04$	$1.07 \pm .04$	$1.53 \pm .17$
Final Hadrons	$1.33 \pm .04$	$1.07 \pm .02$	$1.05 \pm .03$	$1.22 \pm .04$

Figure Captions

Figure 1. 3-jet event structure for (a) SF, (b) IF and (c) CF models. In (a) and (b), the arrows indicate the momentum space distribution of particles. The dashed curves in (a) represent strings stretched between the partons, in (b) they represent the parton directions. (c) shows the CF model quark-gluon shower (solid and curly lines) and clusters (dotted ellipses). The motion of the clusters is indicated by arrows; the resulting momentum space distribution of particles is similar to that in (a) for CF models exhibiting a depletion effect (see text).

Figure 2. Multi-parameter fit results for the SF and IF_1 models. The values of α_S and σ_q predicted by the 40 combinations of distributions used to constrain the parameters are shown for each model. A typical 1σ statistical error is displayed for an SF point, in solid black.

Figure 3. Particle density distribution $(1/N)\ dN/d\phi$ in 3-jet events for (a) all charged particles and photons, for (b) those charged particles and photons satisfying $0.3 < p_{out} < 0.5$ GeV and for (c) a heavy particle sample of charged and neutral kaons, protons and lambdas. Also shown are the predictions of the SF, IF_1 and CF models with full detector simulation.

Figure 4. The ratio $\mathcal{N}_{31}/\mathcal{N}_{12}$ of the normalized particle populations between jets, for the data and models with full detector simulation. (a) and (b) show $\mathcal{N}_{31}/\mathcal{N}_{12}$ for charged pions in two intervals of p_{out}: $0.0 < p_{out} < 0.2$ GeV (a) and $0.3 < p_{out} < 0.5$ GeV (b). (c) and (d) show $\mathcal{N}_{31}/\mathcal{N}_{12}$ for all charged pions and for the heavy particle sample of figure 3(c), respectively.

Figure 5. Q_1 distribution, corrected for detector acceptance and initial-state radiation, compared to the prediction of the SF model (solid curve). The dashed curve shows the shape of the Q_1 distribution, in arbitrary units, for 4 parton events with a minimum parton-parton invariant mass of 7 GeV.

Figure 6. $\Delta M^2_{jet}/E^2_{vis}$ distribution compared to the prediction of the IF_1 model (solid curve). As in figure 5, the data is corrected for detector acceptance and initial-state radiation, and the dashed curve exhibits the shape of the distribution for the 4-parton events, in arbitrary units.

Figure 7. Schematic representation of (a) $q\overline{q}g$ and (b) ggg 3-jet events, in the Webber CF model. The solid line segments indicate color indices: thus quarks are represented by single lines and gluons by double lines. The dotted ellipses represent color singlet clusters. For $q\overline{q}g$ events (a), clusters form between jets 1 and 3 and between jets 2 and 3 but not in the jet 1-2 region. For ggg events (b), clusters form in all the regions between jets.

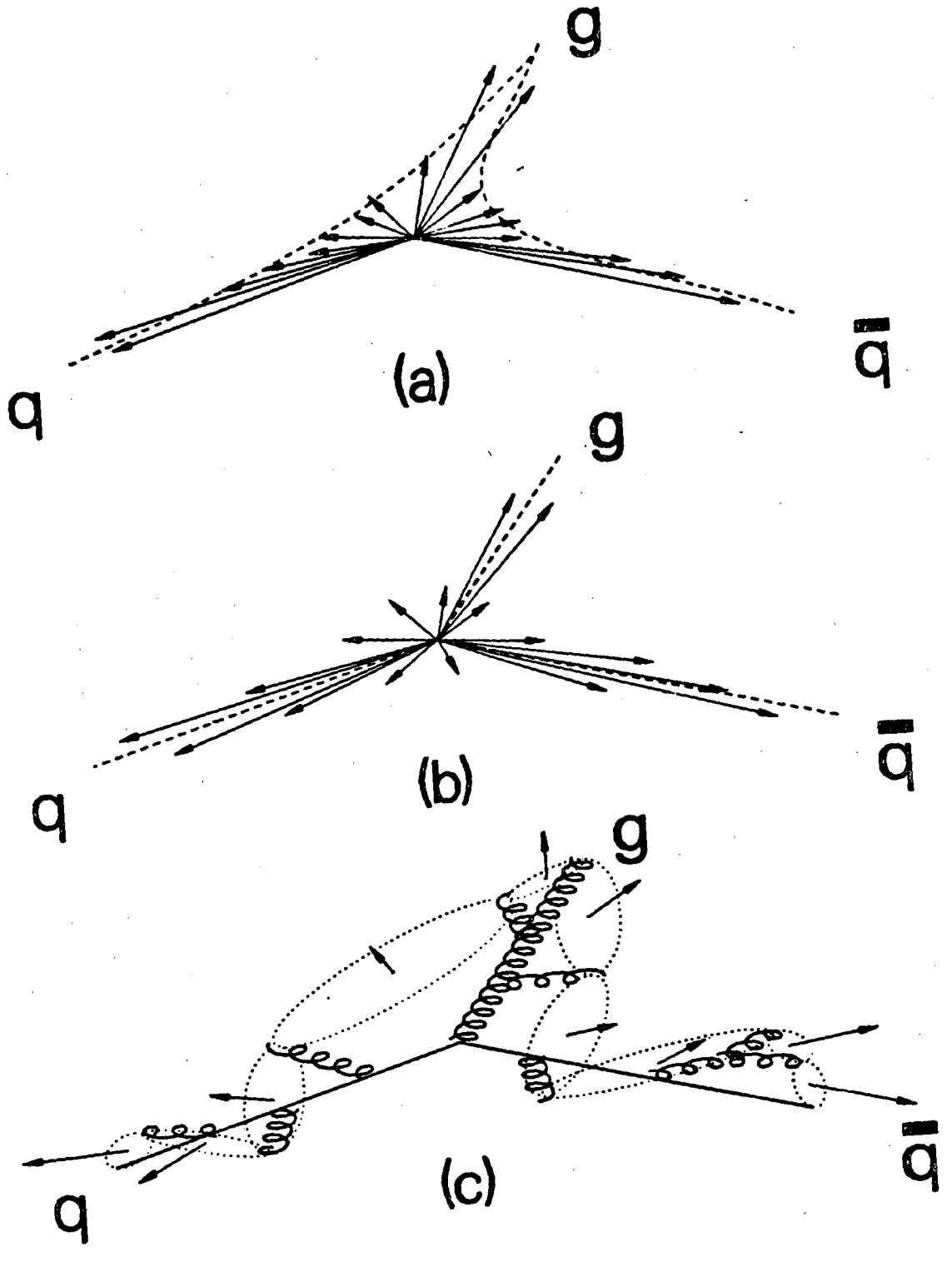

XBL 8410-4316

Figure 1

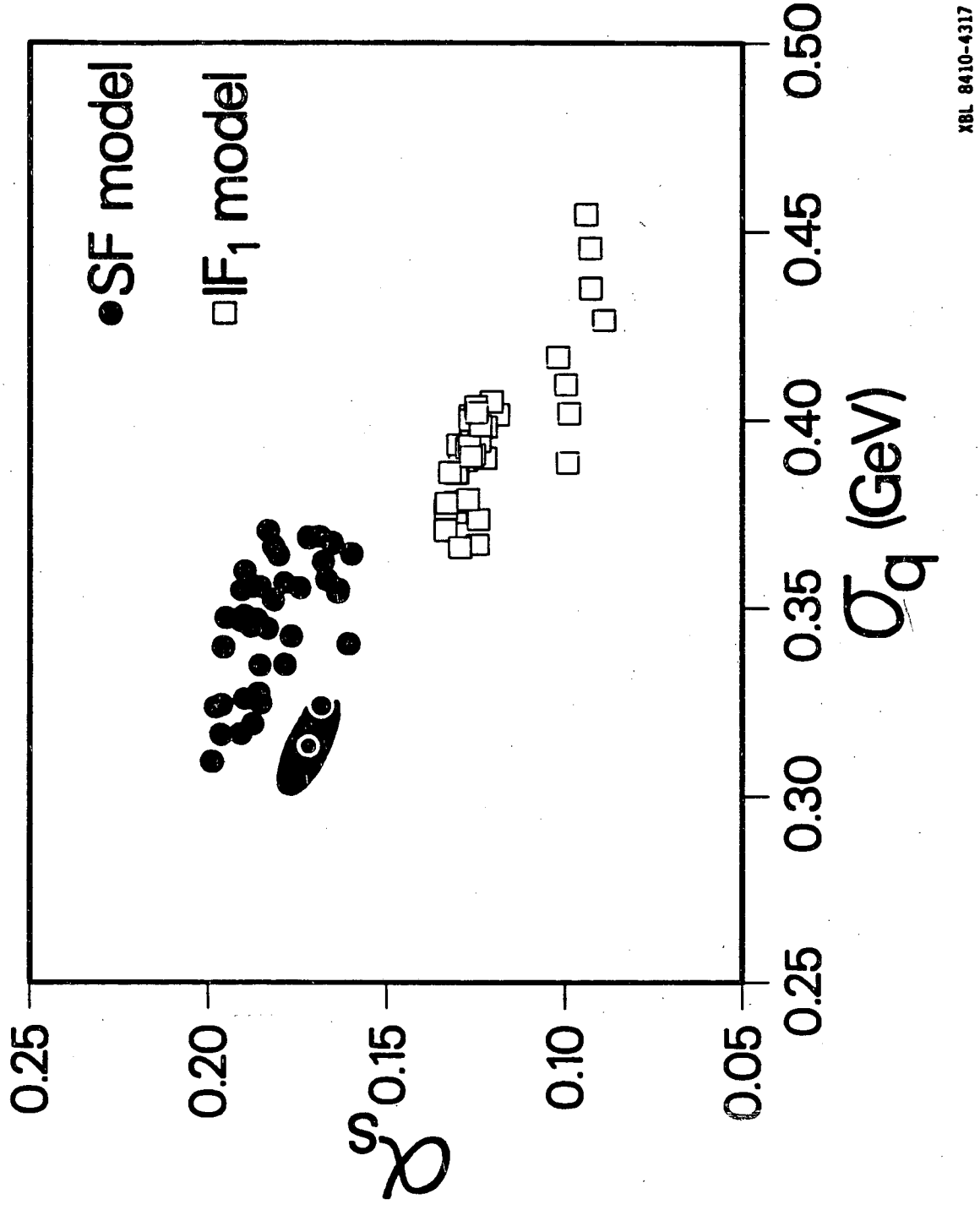

XBL 8410-4317

Figure 2

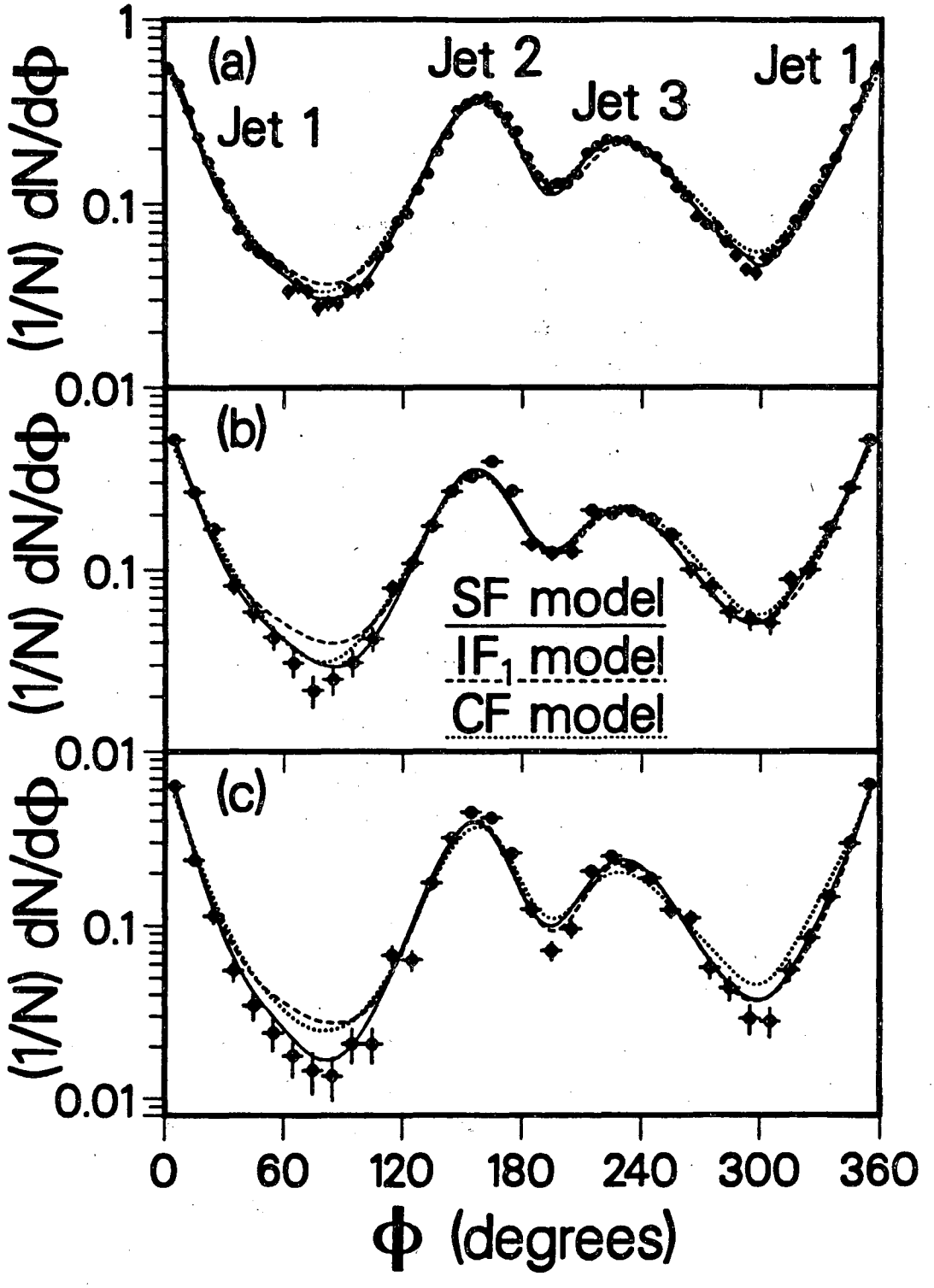

XBL 8410-4318

Figure 3

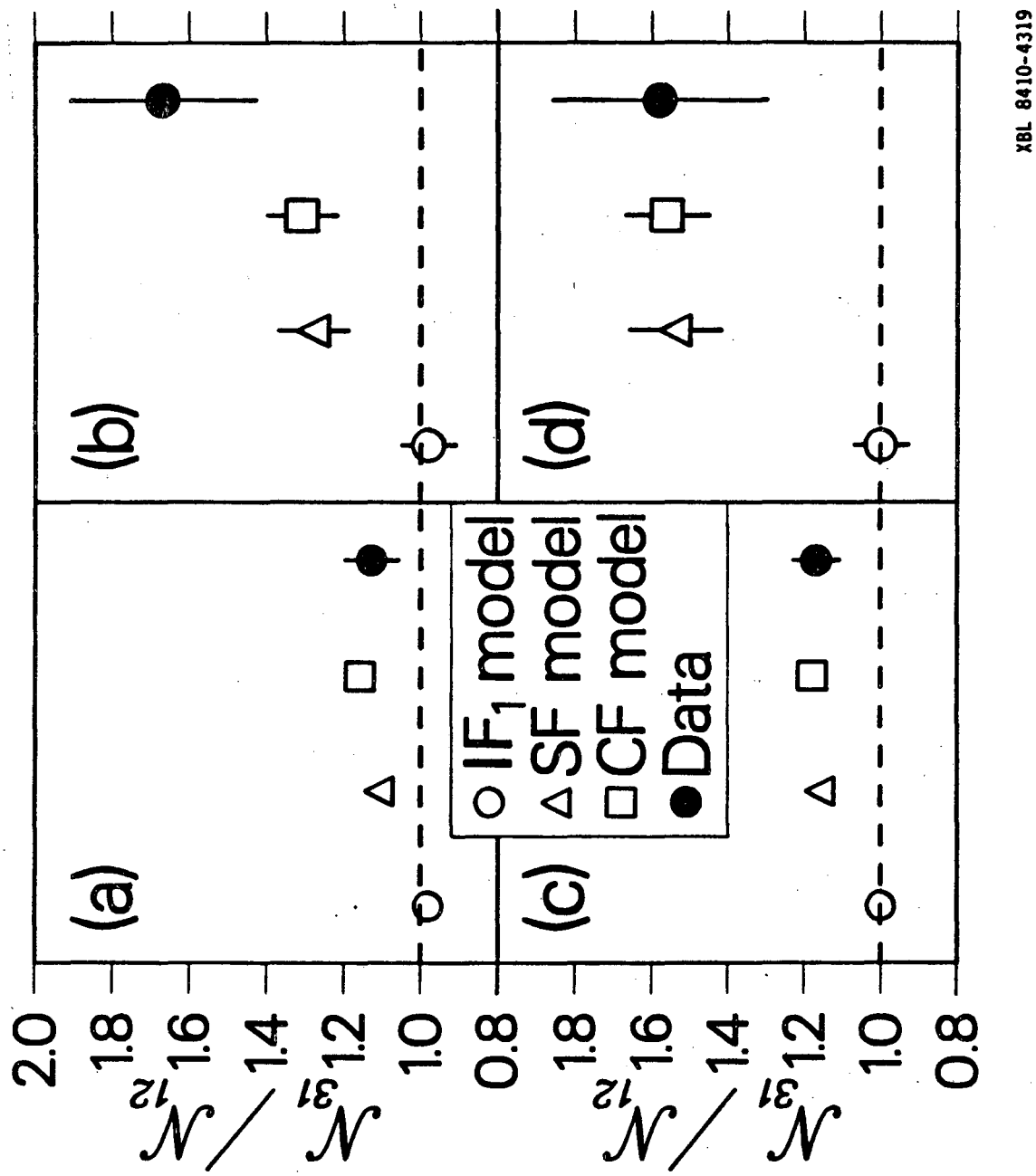
(a)
(b)
(c)
(d)
IF1 model
SF model
CF model
Data
2.0
1.8
1.6
1.4
1.2
1.0
0.8
N31 / N12
XBL 8410-4319

Figure 4

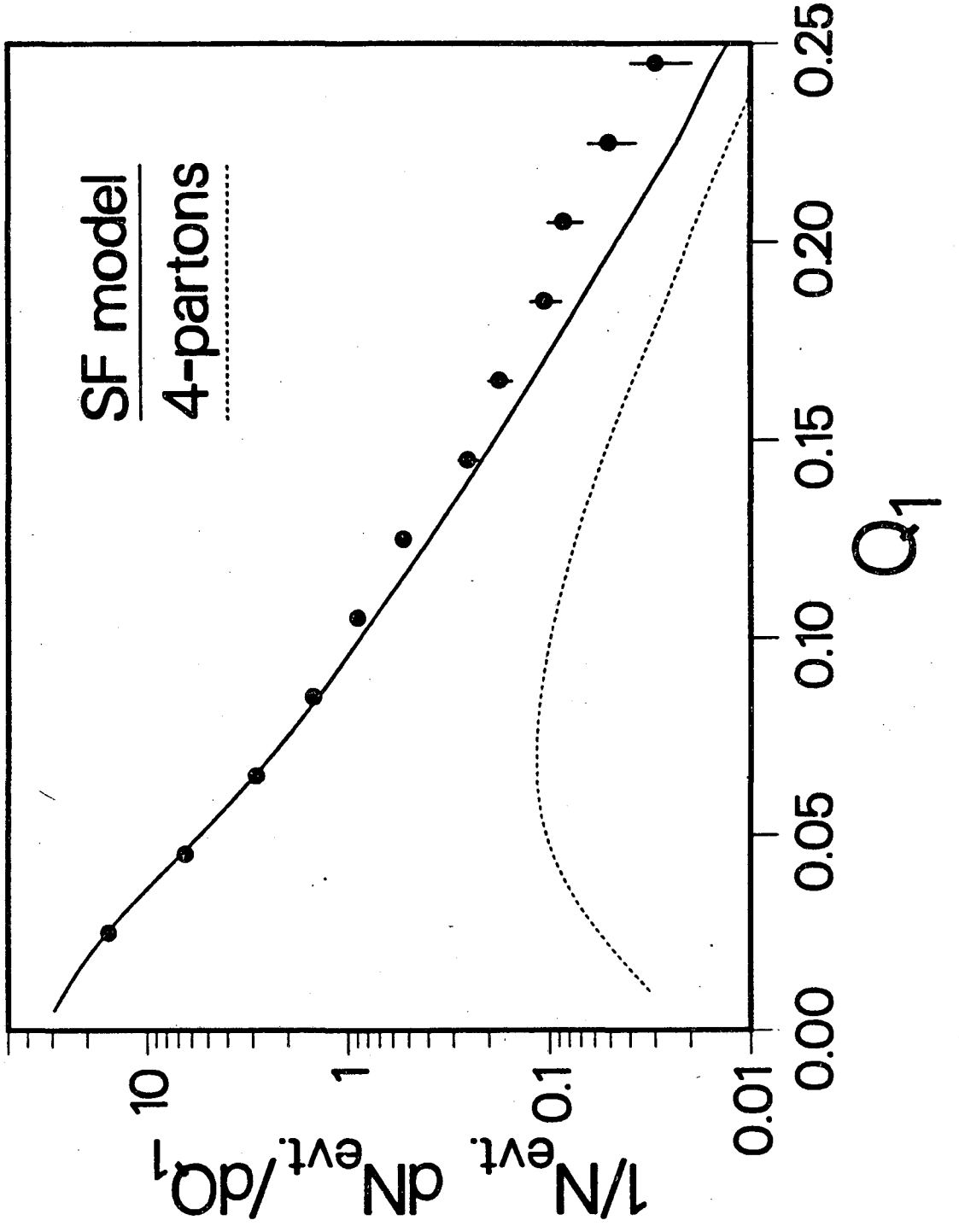

XBL 8410-4320

Figure 5

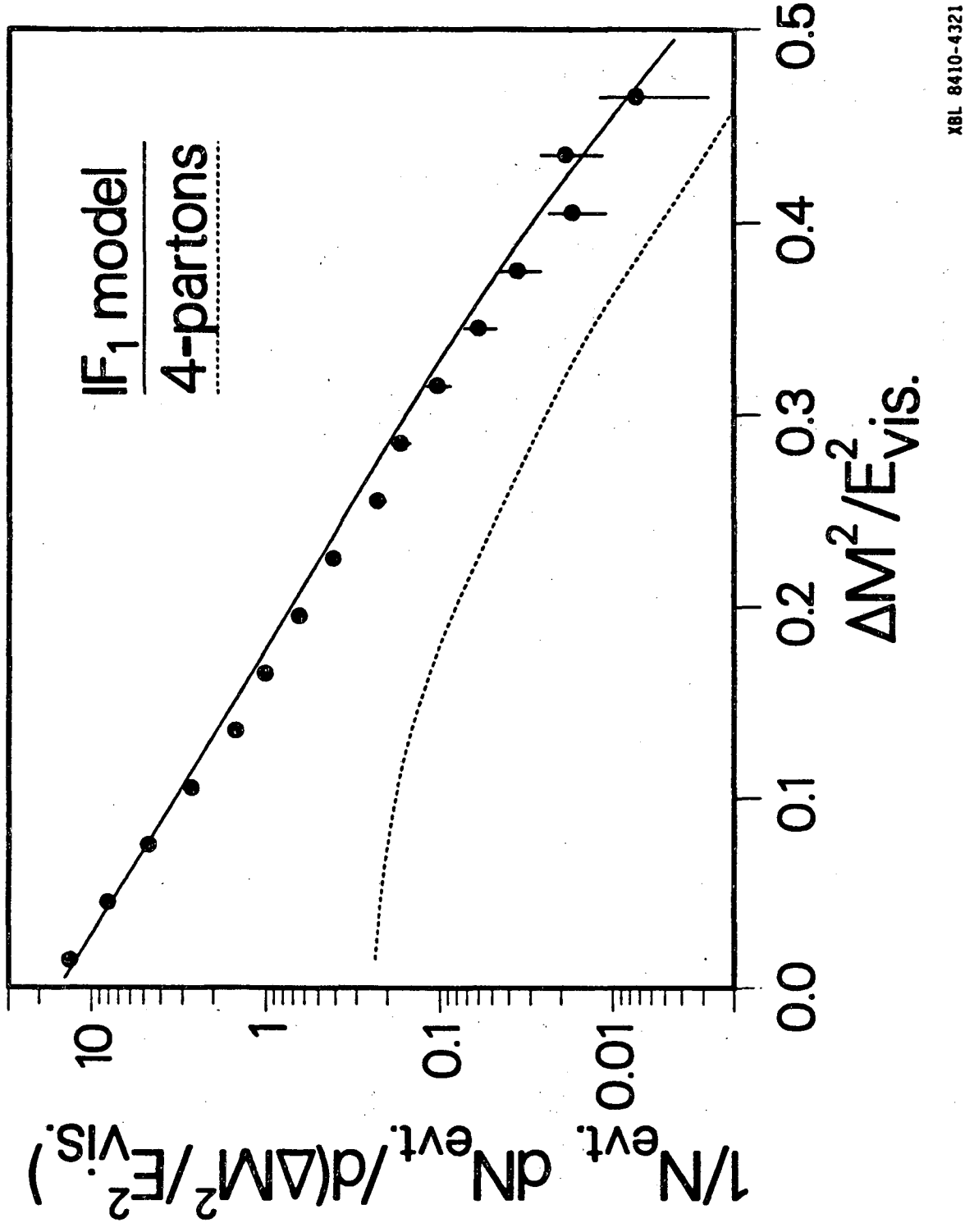

XBL 8410-4321

Figure 6

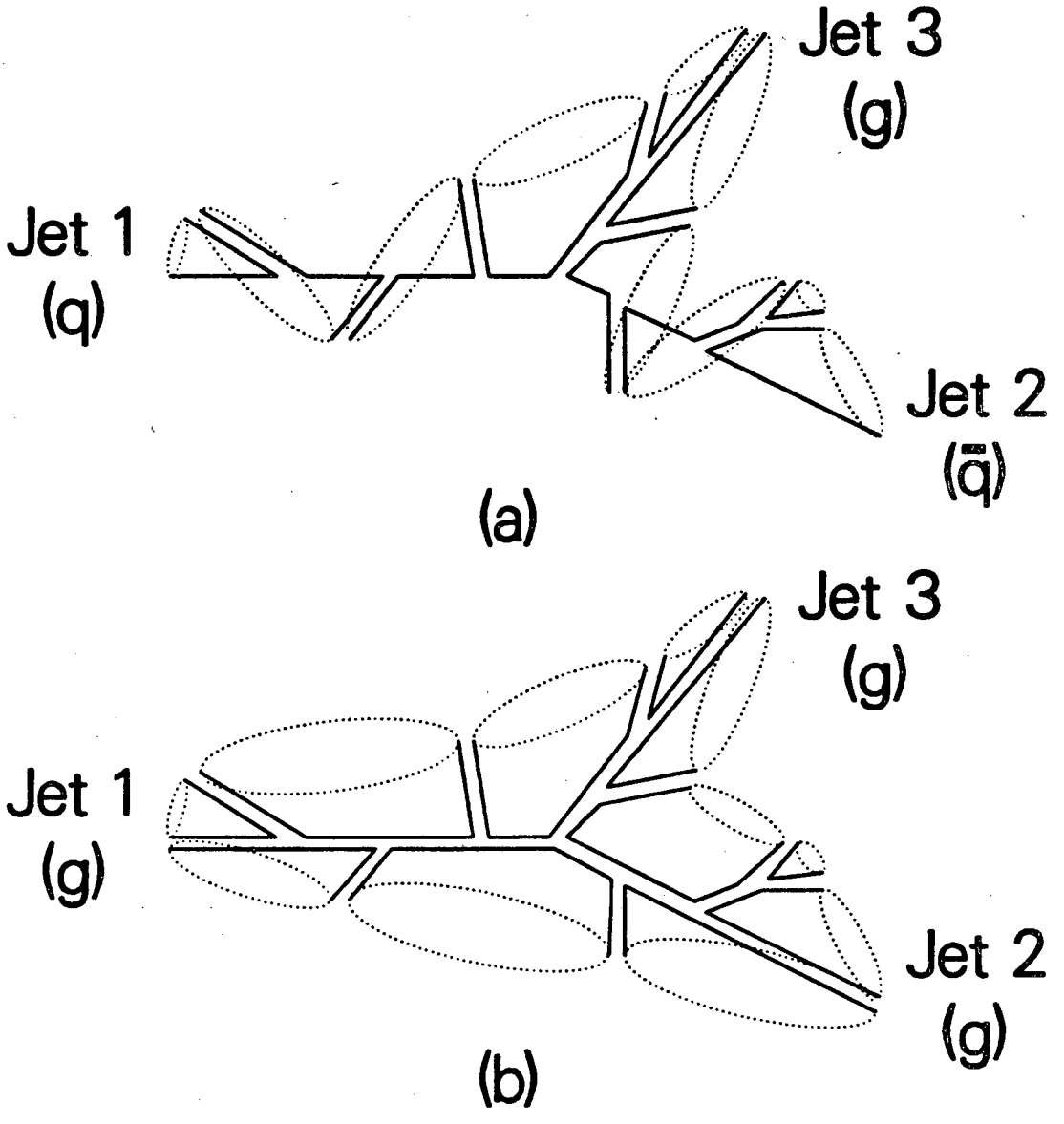

XBL 8410-4322

Figure 7

This report was done with support from the Department of Energy. Any conclusions or opinions expressed in this report represent solely those of the author(s) and not necessarily those of The Regents of the University of California, the Lawrence Berkeley Laboratory or the Department of Energy.

Reference to a company or product name does not imply approval or recommendation of the product by the University of California or the U.S. Department of Energy to the exclusion of others that may be suitable.

TECHNICAL INFORMATION DEPARTMENT
LAWRENCE BERKELEY LABORATORY
UNIVERSITY OF CALIFORNIA
BERKELEY, CALIFORNIA 94720